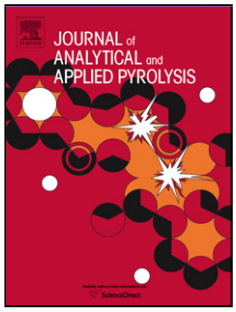

Title: ANALYSIS OF THE VAPORIZATION PROCESS IN TG APPARATUS AND ITS INCIDENCE IN PYROLYSIS

Authors: Rafael Font, M. Francisca Gómez-Rico, Nuria Ortuño

PII: S0165-2370(11)00011-8
DOI: doi:10.1016/j.jaap.2011.01.007
Reference: JAAP 2526

To appear in: *J. Anal. Appl. Pyrolysis*

Received date: 15-7-2010
Revised date: 1-12-2010
Accepted date: 15-1-2011

Please cite this article as: R. Font, M.F. Gómez-Rico, N. Ortuño, ANALYSIS OF THE VAPORIZATION PROCESS IN TG APPARATUS AND ITS INCIDENCE IN PYROLYSIS, *Journal of Analytical and Applied Pyrolysis* (2010), doi:10.1016/j.jaap.2011.01.007

ANALYSIS OF THE VAPORIZATION PROCESS IN TG APPARATUS AND ITS INCIDENCE IN PYROLYSIS

Rafael Font*, M. Francisca Gómez-Rico, Nuria Ortuño
Chemical Engineering Department, University of Alicante, P.O. Box 99, E-03080 Alicante, Spain

Abstract

An analysis of the evaporation process of n-hexadecane in a thermogravimetric apparatus was carried out. N-hexadecane represents a typical example of a high boiling point compound and its study is interesting for understanding those processes where vaporization takes place in parallel with pyrolysis during thermal treatment. The process has been studied under different operating conditions: nitrogen and air atmospheres, and isothermal and dynamic runs with three different heating rates from 5 K/min to 20 K/min. The experimental data were satisfactorily correlated to a n-order model with zero process order and the same apparent activation energy for all runs, but the exponential factors of the different runs depended on the initial mass and the heating rate. The experimental results were compared with those predicted considering the diffusion process inside the crucible, taking into account the vapor pressure and the diffusion coefficient of n-hexadecane. A parameter, product of these two variables, can be estimated from a single TG run, so the vaporization process in other equipment and/or operating conditions can also be estimated.

Keywords: TG; n-hexane; vaporization; kinetic model

1. Introduction

TG and DTA runs, in both dynamic and isothermal configurations, can be useful for obtaining the temperature range of decomposition, decomposition rates and kinetics with the corresponding models and parameters. In TG runs, the weight loss is measured vs. time/temperature, whereas in the DTA endothermic or exothermic processes can be observed. Evaporation is an endothermic process and normally zero-order type for the kinetics of weight loss [1].

* Corresponding author. Tel.: +34 96 590 35 46; fax: +34 96 590 38 26.
E-mail address: rafael.font@ua.es (R. Font)

In many compounds, mixtures and polymers, the decomposition process takes place prior, after or simultaneously to a vaporization process, so the knowledge of the vaporization process, its kinetics and the significance of kinetic parameters are useful.

TBBA is used as a flame retardant in electric circuits, and is present in a significant amount in some electronic wastes. TBBA is a typical example of a compound with high boiling point and vaporization simultaneous to decomposition [2,3].

Polyethylene, polypropylene and polystyrene melt before their pyrolytic decomposition, and vaporization of different products takes place simultaneously to the pyrolysis process [4].

Pyrolysis of oils has been also studied, and an initial vaporization was considered to explain the weight loss observed in the TG runs. In these studies, it was observed that the experimental data were satisfactorily simulated considering the same apparent activation energy with a zero n-order process for all runs, but with pre-exponential factors that depended on the initial mass and the heating rate [5,6].

In many decomposition processes carried out in TG apparatus, the experimental results are not reproducible. The evaporation process may depend on random variables, such as the crucible material an geometry.

The objective of this paper has been to study the evaporation process in a TG instrument. The weight loss has been studied with the criteria widely used for many pyrolytic decompositions, considering zero-order process, due to its simplicity. An analysis of the diffusion process has also been carried out, comparing these results with the experimental values and with the previously simulated results considering the zero-order process. In addition, the parameters that can be obtained from a TG run are discussed for calculating local coefficients of mass transfer in other equipment. Finally, the analysis presented in this paper can also be useful for testing the performance of the TG equipment when used for liquids.

2. Experimental

N-hexadecane supplied by Merck was used in this work.

Runs for pyrolysis and combustion analyses were carried out in a Mettler Toledo thermobalance model TGA/SDTA851e/LF/1600. This apparatus has a horizontal furnace and a parallel-guided balance. In this way, the position of the sample has no influence in the measurement, and flow gas perturbation and thermal buoyancy are

minimized. The sample temperature was measured with a sensor directly attached to the sample holder.

The atmosphere used was nitrogen or air with a flow rate of 100 mL/min, (measured at room temperature).

Dynamic experiments were carried out at heating rates of 5, 10 and 20 K/min, from room temperature up to 600 K. This temperature range included the entire range of vaporization. Isothermal experiments started with a heating rate similar to dynamic experiments until the desired temperature was reached, and the final temperature was kept constant until the vaporization was complete. Different sample masses were used, between 2.5 mg and 10 mg.

An experiment with a heating rate of 5 K/min using Avicel PH-105 microcrystalline cellulose was done. The kinetic values obtained showed good agreement with the results presented by Grønli et al.[7] in their round-robin study of pyrolysis kinetics of cellulose by thermogravimetry. This experiment was used to check performance of the thermobalance.

3. Experimental results

Figure 1 shows the experimental results corresponding to the dynamic runs carried out in nitrogen atmosphere with approximately 9 mg and at three heating rates. In this figure and the following ones, the weight fraction is plotted vs. temperature (the weight fraction represents the non-volatilized fraction). DTA for the 20 K/min run is also plotted, where an endothermic peak can be observed at the last part of the weight loss curve. It can be observed that the curves move to the right when the heating rate increases, as occurs in most pyrolysis reactions. The latter is a consequence of the kinetic law (at high heating rates the decomposition time at low temperature is less than at low heating rate). The end of the endothermic peak corresponds to nearly total evaporation at 513 K and 20 K/min, before the boiling point of hexadecane (560 K). It can also be observed that the curves cross at the beginning of the decompositions, which can only be explained by random factors that can modify the evaporation process.

Figure 1

Figures 2 to 4 show the TG experimental results carried out with 9 mg above mentioned together with their DTG results. It can be pointed out that these figures also show the calculated curves obtained with the models studied, but they will be discussed

in the following section. In Figure 2, there is a small wide peak at 382 K in the DTG curve, which does not appear in all runs. It could indicate the presence of small irregularities in the vaporization process. The tendencies of variation for both curves (weight fraction and DTG) are similar in all tests.

Figures 2 to 4

Figures 5 to 7 show the evaporation runs in air atmosphere, with similar results to the previous ones corresponding to the nitrogen runs.

Figures 5 to 7

The runs corresponding to an initial mass around 5 mg are shown in Figures 8 to 10. It can be observed that there is a significant irregularity in the shape of the curve corresponding to the 5 K/min run. Two more runs with initial mass around 2.5 and 7.5 mg were carried out, and the corresponding results are plotted in Figures 11 and 12, where some irregularities in the shape of the curves can also be observed.

Figures 8 to 12.

The results of three isothermal runs are shown in Figure 13. These runs were carried out at a constant heating rate until reaching the corresponding temperature, and the vaporization process took place at this temperature up to the end of the process. The variation of the weight fraction, after an initial period, is nearly lineal, indicating a nearly constant evaporation rate, as expected. The deviations from linearity, mainly at the end of the process, can be due to the decrease of the evaporation surface, when forming small drops on the bottom of the crucible instead of being extended throughout the entire bottom area.

Figure 13

4. Kinetic models

Before considering the two models presented in this paper, it must be stated that due to some random factors, the kinetic models cannot be exact. They can be useful however to obtain an approximation to the actual phenomena.

The vaporization process takes place as a consequence of the vapor diffusion from the liquid surface at the bottom of the crucible. Any factor that can alter one of the variables evolved can modify the evaporation rate. Among these parameters, there can be the surface of the liquid at the crucible bottom, the type of diffusion (molecular or convective), heat transport, some irregularities of the crucible (bottom and side walls), etc.

4.1 Correlation model

The process can be described as

$$\text{n – hexadecane (liquid)} \xrightarrow{1} \text{n – hexadecane (vapor)}$$

The conversion degree α can be defined as the ratio between the mass fraction of volatiles obtained at any time during which the process is taking place (v) and the maximum possible (v_∞)

$$\alpha = \frac{v}{v_\infty} \tag{1}$$

The kinetic equation, considering the conversion degree , is as follows:

$$\frac{d\alpha}{dt} = k(1-\alpha)^{n_1} \tag{2}$$

The kinetic constant can be expressed by the Arrhenius law as:

$$k = k_o \exp\left(-\frac{E}{RT}\right) \tag{3}$$

By numerical integration of these equations, it is possible to calculate α at any time if the temperature program is known. The mathematical procedure was the Euler method, but with very small increments of time, and in accordance with the experimental variation of temperature vs. time. It was tested that the errors produced by the size of the intervals were negligible (considering small intervals). The optimization program used for obtaining the best set of kinetic parameters was based on minimizing the difference between the experimental curves and those calculated by integration of the previous differential equations.

Initially the parameters considered for optimization of a single run were the pre-exponential factor, the activation energy and the process order, in accordance with the procedure explained in the following paragraphs. The optimized value of the process order was close to zero. Normally, the vaporization process is correlated with nil or very small process order, so this parameter was fixed to zero and the kinetic equation can be expressed as:

$$\frac{d\alpha}{dt} = k_o \exp\left(-\frac{E}{RT}\right) \tag{4}$$

On the other hand, it was deduced that acceptable correlations of the experimental data were only obtained when the pre-exponential factor was considered different for each run, whereas the apparent activation energy was the same for all runs. Remember that the maximum value of vaporized mass equals 1 and the process order is 0 for all runs. In the correlation of the pyrolysis data of oils from Gómez-Rico et al. [5] and Fuentes et al. [6], different values of the pre-exponential factor for each run were also considered. Consequently, the parameters optimized for the 14 runs were 14 pre-exponential factors and the apparent activation energy.

The objective function (OF) to minimize was the sum of the squares of the difference between experimental and calculated weight fraction values of n-hexadecane remaining as a liquid on the thermobalance[P1], inside the interval of variation:

$$OF = \sum_{m=1}^{3}\sum_{j=1}^{N}(w_{mj}^{\exp} - w_{mj}^{cal})^2 \quad \text{m heating rates, j points (5[P2])}$$

The model validity has been tested calculating the variation coefficient (VC):

$$VC = \frac{\sqrt{OF/(N-P)}}{\overline{w}_{exp}} x100 \qquad (6)_{[P3]}$$

where N and P are the number of data and parameters fitted, respectively, and $\overline{w_{exp}}$ is the average of the experimental weight fractions.

The results of the optimized parameters are presented in Table 1: apparent activation energy and the 14 values of k_o. For each run, the variation coefficient VC was determined and an average value VC is also presented. Figures 1 to 14 show the calculated curves by integration of the differential equations. The experimental data are plotted with a solid line, whereas the calculated curves by this method correspond to the thin line (cal1). An acceptable correlation for all data was observed. A small deviation was detected in the isotherm run carried out with the 5 K/min heating rate.

Table 1

A variation of the pre-exponential factor vs. the heating rate and the initial mass was observed. Considering the vaporization process, an inverse variation of the pre-exponential factor vs. the initial mass is acceptable, whereas the dependence on the heating rate should be nil. The relation obtained between the optimized values of the pre-exponential factors, the initial mass and the heating rate can be seen in Figure 14. An acceptable correlation can be observed, but inside a wide scattering of the points.

The exponents 0.5 for the heating rate and -1 for the initial mass were obtained by minimizing the differences between optimized pre-exponential factors and correlated ones (in fact, the exponents obtained were 0.49 and -0.98 respectively). The relation deduced is:

$$k_o(s^{-1}) = 261.9 \ \text{heating rate}^{-0.5}((^oC/\min)^{-0.5}) \ m_o^{-1}(mg^{-1}) \quad (7)$$

Using the previous expression, the values of the pre-exponential factor were calculated (k_o cal), and these values and the variation coefficient, considering the experimental and calculated values of weight fractions, are also presented in Table 1. An average value of the variation coefficient around 12 % is obtained, indicating that the correlation of the data, although acceptable, is not very good.

Figure 14

4.2 Vaporization model

A vaporization model has been developed, considering the cylindrical geometry of the crucible, and that the vaporization process is controlled by the molecular diffusion of n-hexadecane through nitrogen (or air, accepting that the diffusion process is similar and there are no oxidation reactions in the temperature range). The driving force is the difference between the vapor pressure in contact with the liquid at the bottom of the crucible and zero or very small pressure at the top of the crucible due to the dilution/drag of the vaporized solvent by the surrounding atmosphere.

The diffusion equation representative of the process is the following:

$$N_A = F\frac{A_c D_o}{LRTy_{air,ml}}(T/T_o)^{1.5}P_v^o = F\frac{A_c D_o}{LRy_{air,ml}}(1/T_o)^{1.5}T^{0.5}P_v^o \quad (8)$$

where N_A is molar flow (mol/s), A_c is the cross sectional area of the crucible (internal diameter $4.6\cdot10^{-3}$ m), D_o is the diffusion coefficient ($1.51\cdot10^{-5}$ $m^2/s_{[P4]}$ at T_o 553.1 K), L is the height from the level of the liquid to the top of the crucible (the height of the crucible is $4.6\cdot10^{-3}$ m) , T is the absolute temperature, R is the gas constant, $y_{air,ml}$ is the logarithmic mean value between the molar fraction of air or nitrogen on the liquid surface and 1 at the top of the crucible, and P_v^o is the vapor pressure that can be calculated by the Antoine Equation:

$$\log_{10} P_v^0(\text{mm Hg}) = 7.0287 - \frac{1830.51}{T(^oC) + 154.45} \quad (9)$$

Other similar expressions for P_v^o have been used, but the simulated results were similar.

A factor F has been introduced for correction of the theoretical simulations, due to possible deviations of concentration gradient, small convection fluxes, deviations of the thermodynamic data, deviations of the liquid surface from linear horizontality, etc.

Initially the factor F was considered to be equal to unity, and acceptable results were obtained for some runs. Table 1 indicates the variation coefficient for each run (when F equals 1), observing small values when the initial mass is around 9 mg, and larger values when the initial mass is smaller than 7.5 mg.

The factor F was optimized for each run, and the variation coefficients are lower than in the previous case (see Table 1). Figures 1 to 14 show the calculated results (line cal2), observing a coincidence with the experimental data in the cases with initial mass around 9 mg.

This factor F has been correlated with the initial mass and the heating rate, observing a poor correlation (Figure 15). The exponents were obtained by minimizing the objective function sum of the squares of the difference between F values optimized and calculated by the n-order equation. With the correlation obtained, new values were obtained for each run, and the variation coefficients were calculated, with an average value around 18 %, indicating a poor correlation.

Consequently, it can be deduced that most of the results obtained with around 9 mg are close to those predicted by the diffusion equation, whereas the other runs significantly differ from the theoretical equation. In general, it seems that the vaporization rate is influenced by random factors that cause a poor correlation of the experimental data. On the other hand, inside this random behavior, it seems that relatively high heating rates cause higher volatilization rates than those calculated, probably due to the influence of convection diffusion caused by greater rates of temperature increase. This possible influence of the heating rate can be also observed for the correlation deduced in the previous model, where the pre-exponential factor has a dependence on the square of the heating rate.

5. Deduction of useful kinetic parameters from the TG data

From the TG data, it is possible to deduce kinetic parameters that correlate the experimental data, but only useful for this crucible used and for the initial mass considered. With the analysis presented in this section, an estimation of the kinetic coefficients important to test the thermobalance performance or to obtain useful information for other operating conditions can be obtained from the data deduced from TG.

A previous aspect that can be considered is the physical meaning of the apparent activation energy obtained in the correlation of the data by TG with the first model considered (42 kJ/mol).

The variation of the vaporization degree can be related to the molar vaporization flow N_A by the equation

$$\frac{d\alpha}{dt} = \frac{N_A M}{m_o} \tag{10}$$

where M is the molecular weight of n-hexadecane.

From the previous equations, it can be deduced that

$$\frac{d\alpha}{dt} = k_o \exp\left(-\frac{E}{RT}\right) = \frac{N_A M}{m_o} = \frac{M}{m_o}\frac{FA_c D_o}{LRy_{air,ml}}(1/T_o)^{1.5} T^{0.5} P_v^o \tag{11}$$

Figure 15

Consequently, the value of the apparent activation energy should correspond to the slope for the variation of logarithm of $T^{0.5}P_v^o/y_{air,ml}$ vs. 1/T. The $y_{air,ml}$ values depend on the temperature and vary between 1 and 0.82 for the runs at 20 ºC/min, between 1 and 0.92 for the runs at 10 ºC/min, and between 1 and 0.95 for the runs at 5 Cº/min. Figure 16 shows the variation of the product of $T^{0.5}P_v^o$ in the temperature range of the vaporization process. A good exponential variation is obtained with a value of E/R equal to 7985 K, corresponding to an apparent activation energy of 65.6 kJ/mol. Figure 17 shows the variation of the term $T^{0.5}P_v^o/y_{air,ml}$ vs. 1/T corresponding to the variation of a run carried out at 20 ºC/min. In this latter case the correlation is very good, the term E/R equals 8266 K, and the apparent activation energy is 67.9 kJ/mol.

These small values of apparent activation energy (65-69 kJ/mol) correspond to the vaporization + diffusion process, and are greater than the value of 41.2 kJ/mol, obtained from the correlation model. The vaporization enthalpy at 1 atm is 80-81 kJ/mol, but at a

pressure lower than 1 atm, as occurs in the vaporization process in the TG, the vaporization enthalpy is lower, around 64 kJ/mol (value that can be obtained from (9)). The apparent activation energy deduced from the correlation model (41.2 kJ/mol) is consistent with the fact that there is no chemical reaction in the temperature range of vaporization.

Figures 16 and 17

Considering that

$$\frac{T^{1/2} P_v^o}{y_{air,ml}} = Q \exp\left[-\frac{E}{RT}\right] \quad \text{[P5]} \qquad (12)$$

where Q is another pre-exponential factor.

From eqs. (11) and (12), it can be deduced that the pre-exponential factor k_o, when F is considered to be unity, equals

$$k_o = \frac{M}{m_o} \frac{A_c D_o}{L R_1} (1/T_o)^{1.5} Q \qquad (13)$$

Assuming that the best results are obtained when the weight loss rate is high, the run carried out with nitrogen at 10 K/min is selected for the extrapolation of the data obtained with TG to other operating conditions. Considering only this run, the best kinetic parameters obtained by the correlation model indicated by eqs. (11) and (13) are:

$k_o = 1.102 \times 10^3\ s^{-1}$

E/R = 7245 K, E= 60.2 kJ/mol

VC= 0.7 %

In this case, the apparent activation energy is close to the theoretical value, and the variation coefficient is very low. Practically the experimental and calculated curves of the vaporization degree vs. temperature overlap each other. Therefore, this method is also useful for analysing the TG apparatus performance with a single run.

With respect to another scale, the vaporization model is useful to obtain important parameters, as follows. Most of the correlations in literature considering local convective transfer coefficients without chemical reaction are based on three non-dimensional numbers:

$$Sh = a\, Re^b\, Sc^c \qquad (14)$$

where the Sherwood number Sh equals

$$Sh = \frac{k_c d_p y_{air,ml}}{D} \tag{15}$$

and where k_c is the local transfer coefficient, d_p is the diameter or another characteristic length, $y_{air,ml}$ is the logarithmic mean value between the molar fraction of air or inert gas on the liquid surface and in the surroundings and D is the diffusivity.

The Reynolds number equals

$$Re = \frac{\rho V d_p}{\mu} \tag{16}$$

where ρ, V and μ are the density, velocity and viscosity of the surrounding fluid respectively.

The Schmidt number Sc equals

$$Sc = \frac{\mu}{\rho D} \tag{17}$$

Normally, the influence of the Schmidt number is small because the exponent c is lower than 0.5.

Considering a convective diffusion with concentration gradient similar to that of the TG crucible (between saturation concentration and zero), the mass flux J_A equals

$$J_A = N_A M = k_c (C_{Ao} - 0) M = k_c \frac{P_v^o}{RT} M = \frac{ShD}{d_p y_{air,ml}} \frac{P_v^o}{RT} M = \frac{ShD_o (T/T_o)^{1.5} M P_v^o}{d_p y_{air,ml} RT}$$
$$= \frac{Sh}{d_p} \frac{D_o (1/T_o)^{1.5} MQ}{y_{air,ml} R} \exp\left[-\frac{E}{RT}\right] \tag{18}$$

Considering eq. (11), it can be deduced that

$$\frac{D_o (1/T_o)^{1.5} MQ}{y_{air,ml} R} = \frac{k_o m_o L}{A_c} \tag{19}$$

For the case considered, L equals 0.0046 m, A_c equals 1.66×10^{-5} m^2, m_o equals 9.3×10^{-6} kg, k_o equals 1.101×10^4 s^{-1}, and consequently

$$\frac{D_o (1/T_o)^{1.5} MQ}{y_{air,ml} R} = \frac{k_o m_o L}{A_c} = 26.07 \ \text{kg/m s}$$

Therefore

$$J_A = N_A M = k_c (C_{Ao} - 0) = \frac{Sh}{d_p} \frac{D_o (1/T_o)^{1.5} MQ}{y_{air,ml} R} \exp\left[-\frac{E}{RT}\right] = \frac{Sh}{d_p} 26.07 \exp\left[-\frac{7245}{T}\right] \quad (20)$$

J_A in kg/sm^2; T in K and d_p in m.

The Sherwood number must be calculated with the Reynolds number and the Schmidt number, where an approximated value of diffusivity must be considered.

Consequently, an estimation of the mass transfer in some cases (with a zero concentration of n-hexane in the surrounding atmosphere) can be obtained by the kinetic results deduced from the correlation of the TG data assuming a zero-order weight loss process. Otherwise, for cases with a concentration of solvent different than zero far from the vaporization surface, the value of diffusivity should be estimated, so as to obtain the other parameters. Nevertheless, this study is useful to obtain some information about the process in spite of the fact that vaporization is a random phenomenon whose kinetic parameters calculated for TG are only applicable to this exact apparatus.

When TG runs are not reproducible, the apparent activation energy is inside the range of that of the vaporization enthalpy and the apparent kinetic constant depends on the heating rate, one can deduce that a vaporization process can be responsible for this behavior.

6. Conclusions[P6]

The kinetics of the vaporization process have been studied. Two kinetic models have been compared, one with process order that equals zero, which is simple and widely used for this kind of process, and another more rigorous, considering the diffusion process. The results obtained are not coincident in some cases due to difficulties related to the random phenomenon.

It must be emphasized that the zero-order potential method is only useful for indicating that there is a vaporization process, but the kinetic constant cannot be used in other apparatuses.

This study also presents a method for testing the thermobalance performance for liquid vaporization, considering the diffusion process. In the positive cases, where the results are reproducible and the vaporization process takes place in accordance with the diffusion law, useful information from results of vaporization TG runs can be applicable

to other operating conditions. In other cases, the information obtained should be properly used, taking into account the random phenomena.

Appendix A: Notation

A_c cross sectional area of the crucible (m^2)

C_{A0} saturation concentration of n-hexadecane (kg/m^3)

D diffusion coefficient (m^2/s)

D_0 diffusion coefficient at T_0 (m^2/s)

d_p diameter or another characteristic length (m)

E apparent activation energy (J/mol)

F correction factor (dimensionless)

J_A mass flux of n-hexadecane ($kg/s\ m^2$)

k kinetic constant (s^{-1})

k_0 pre-exponential factor (s^{-1})

k_c local transfer coefficient (m/s)

L height from the liquid surface to the top of the crucible (m)

M molecular weight of n-hexadecane (kg/mol)

m_0 initial sample mass (kg)

n_1 process order (dimensionless)

N_A molar flow of n-hexadecane (mol/s)

P_v^0 vapor pressure of n-hexadecane (Pa)

Q pre-exponential factor [P7]($K^{0.5}$ Pa)

R gas constant (J/mol K)

Re Reynolds number (dimensionless)

Sc Schmidt number (dimensionless)

Sh Sherwood number (dimensionless)

T temperature (K)

T_0 reference temperature (K)

v mass fraction of volatiles (dimensionless)

V velocity of air or inert gas (m/s)

v_∞ maximum mass fraction of volatiles (dimensionless)

VC variation coefficient (dimensionless)

w weight fraction of the material remaining on the crucible (dimensionless)

$y_{air, ml}$ logarithmic mean value between the molar fraction of air or inert gas on the liquid surface and the top of the crucible (dimensionless)

Greek letters

α conversion degree (dimensionless)

μ dynamic velocity of air or inert gas (Pa s)

ρ density of air or inert gas (kg/m^3)

Acknowledgements[P8]

Support for this work was provided by PROMETEO/2009/043/FEDER and ACOMP2010/075 of Generalitat Valenciana (Spain) and CTQ2008-05520 (Spanish MCI /research).

References

[1] A. Hazra, D. Dollimore, K. Alexander, Thermal analysis of the evaporation of compounds used in aromatherapy using thermogravimetry, Thermochim. Acta 392-393 (2002) 221-229.

[2] A. Marongiu, G. Bozzano, M. Dente, E. Ranzi, T. Faravelli, Detailed kinetic modeling of pyrolysis of tetrabromobisphenol A, J. Anal. Appl. Pyrol. 80 (2007) 325-345.

[3] F. Barontini, V. Cozzani, K. Marsanich, V. Raffa, L. Petarca, An experimental investigation of tetrabromobisphenol A decomposition pathways, J. Anal. Appl. Pyrol. 72 (2004) 41-53.

[4] A. Marongiu, T. Faravelli, E. Ranzi, Detailed kinetic modeling of the thermal degradation of vinyl polymers, J. Anal. Appl. Pyrol. 78 (2007) 343-362.

[5] M. F. Gómez-Rico, I. Martín-Gullón, A. Fullana, J.A. Conesa, R. Font, Pyrolysis and combustion kinetics and emissions of waste lube oils, J. Anal. Appl. Pyrol. 68-69 (2003) 527-546.

[6] M.J. Fuentes, R. Font, M.F. Gómez-Rico, I. Martín-Gullón, Pyrolysis and combustion of waste lubricant oil from diesel cars: Decomposition and pollutants, J. Anal. Appl. Pyrol. 79 (2007) 215-226.

[7] M. Grønli, M.J. Antal, G. Várhegyi, A round-robin study of cellulose pyrolysis kinetics by thermogravimetry, Ind. Eng. Chem. Res. 38 (1999) 2238-2244.

Table 1. Kinetic parameters of the correlation models

			Zero-order model Apparent activation energy = 41.2 kJ/mol				Vaporization model Case F=1		Case F optimized		Case F correlated	
Run	**K/min**	**m_0 (mg)**	**$k_o(s^{-1})$ opt.**	**VC (%)**	**$k_o(s^{-1})$ cal.**	**VC (%)**	**F**	**VC (%)**	**F opt.**	**VC (%)**	**F cal.**	**VC (%)**
N_2 dynamic	20	9.05	93.8	6.9	126.2	19.3	1.00	7.2	0.87	4	1.46	21.5
N_2 dynamic	10	9.30	70.8	8.5	86.8	15.4	1.00	7.4	0.85	2	1.37	20.3
N_2 dynamic	5	9.05	62.4	7.0	63.1	7.1	1.00	6.3	0.93	5.6	1.33	15.6
Air dynamic	20	9.13	99.8	6.3	125.1	15.3	1.00	4.7	0.96	4.4	1.45	17.8
Air dynamic	10	9.49	92.4	2.0	85.1	5.4	1.00	15.9	1.30	11.2	1.35	11.3
Air dynamic	5	9.56	70.7	1.3	59.7	10.4	1.00	15.2	1.28	11	1.28	11
N_2 dynamic	20	5.22	286.8	3.1	218.8	16.4	1.00	47.8	3.14	14.1	2.06	22
N_2 dynamic	10	4.85	190.3	5.1	166.4	9.1	1.00	36.0	2.24	16	2.05	16.3
N_2 dynamic	5	4.81	165.1	12.7	118.8	22.8	1.00	45.6	2.78	24.5	1.96	27.4
N_2 isothermal	20	9.25	122.4	5.0	123.4	5.1	1.00	38.7	1.68	9.4	1.44	16.3
N_2 isothermal	10	9.15	94.8	7.1	88.2	9.1	1.00	46.3	1.80	11.1	1.38	23.4
N_2 isothermal	5	9.63	44.1	7.7	59.3	24.5	1.00	19.2	1.22	8.9	1.28	9.7
N_2 dynamic	10	2.48	299.0	8.2	326.2	9.6	1.00	41.2	2.49	20.4	3.11	28
N_2 dynamic	10	7.58	104.4	4.4	106.6	4.6	1.00	16.2	1.27	12.7	1.55	14.8
Mean value				6.1		12.4		24.8		11.1		18.2

FIGURE CAPTIONS

Figure 1. Variation of the weight fraction and DTA vs. temperature in N_2 atmosphere (sample mass: 9 mg).

Figure 2. Experimental and calculated data for TG and DTG in N_2 atmosphere (sample mass:9 mg, 20 K/min)

Figure 3. Experimental and calculated data for TG and DTG in N_2 atmosphere (sample mass: 9 mg, 10 K/min)

Figure 4. Experimental and calculated data for TG and DTG in N_2 atmosphere (sample mass: 9 mg, 5 K/min)

Figure 5. Experimental and calculated data for TG and DTG in air atmosphere (sample mass: 9 mg, 20 K/min)

Figure 6. Experimental and calculated data for TG and DTG in air atmosphere (sample mass: 9 mg, 10 K/min)

Figure 7. Experimental and calculated data for TG and DTG in air atmosphere (sample mass: 9 mg, 5 K/min)

Figure 8. Experimental and calculated data for TG and DTG in N_2 atmosphere (sample mass: 5 mg, 20 K/min)

Figure 9. Experimental and calculated data for TG and DTG in N_2 atmosphere (sample mass: 5 mg, 10 K/min)

Figure 10. Experimental and calculated data for TG and DTG in N_2 atmosphere (sample mass: 5 mg, 5 K/min)

Figure 11. Experimental and calculated data for TG and DTG in N_2 atmosphere (sample mass: 2.5 mg, 10 K/min)

Figure 12. Experimental and calculated data for TG and DTG in N_2 atmosphere (sample mass: 7.5 mg, 10 K/min)

Figure 13. Experimental and calculated data for isothermal runs in N_2 atmosphere (sample mass: 9 mg,)

Figure 14. Variation of the pre-exponential factor vs. initial mass and heating rate

Figure 15. Variation of the factor F vs. heating rate and initial mass

Figure 16. Variation of $T^{0.5}P_v^o$ vs. 1/T.

Figure 17. Variation of $T^{0.5}P_v^o / y_{air,ml}$ vs. 1/T.

.

Table 1. Kinetic parameters of the correlation models

			Zero-order model				Vaporization model					
			Apparent activation energy = 41.2 kJ/mol				Case F=1		Case F optimized		Case F correlated	
Run	**K/min**	**m_0 (mg)**	**$k_o(s^1)$ opt.**	**VC (%)**	**$k_o(s^{-1})$ cal.**	**VC (%)**	**F**	**VC (%)**	**F opt.**	**VC (%)**	**F cal.**	**VC (%)**
N_2 dynamic	20	9.05	93.8	6.9	126.2	19.3	1.00	7.2	0.87	4	1.46	21.5
N_2 dynamic	10	9.30	70.8	8.5	86.8	15.4	1.00	7.4	0.85	2	1.37	20.3
N_2 dynamic	5	9.05	62.4	7.0	63.1	7.1	1.00	6.3	0.93	5.6	1.33	15.6
Air dynamic	20	9.13	99.8	6.3	125.1	15.3	1.00	4.7	0.96	4.4	1.45	17.8
Air dynamic	10	9.49	92.4	2.0	85.1	5.4	1.00	15.9	1.30	11.2	1.35	11.3
Air dynamic	5	9.56	70.7	1.3	59.7	10.4	1.00	15.2	1.28	11	1.28	11
N_2 dynamic	20	5.22	286.8	3.1	218.8	16.4	1.00	47.8	3.14	14.1	2.06	22
N_2 dynamic	10	4.85	190.3	5.1	166.4	9.1	1.00	36.0	2.24	16	2.05	16.3
N_2 dynamic	5	4.81	165.1	12.7	118.8	22.8	1.00	45.6	2.78	24.5	1.96	27.4
N_2 isothermal	20	9.25	122.4	5.0	123.4	5.1	1.00	38.7	1.68	9.4	1.44	16.3
N_2 isothermal	10	9.15	94.8	7.1	88.2	9.1	1.00	46.3	1.80	11.1	1.38	23.4
N_2 isothermal	5	9.63	44.1	7.7	59.3	24.5	1.00	19.2	1.22	8.9	1.28	9.7
N_2 dynamic	10	2.48	299.0	8.2	326.2	9.6	1.00	41.2	2.49	20.4	3.11	28
N_2 dynamic	10	7.58	104.4	4.4	106.6	4.6	1.00	16.2	1.27	12.7	1.55	14.8
Mean value				6.1		12.4		24.8		11.1		18.2

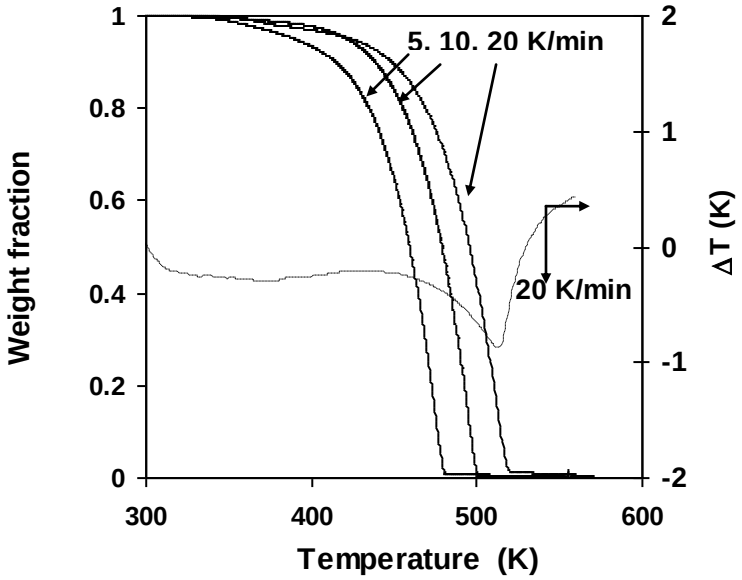

Figure 1. Variation of the weight fraction and DTA vs. temperature in N_2 atmosphere (sample mass: 9 mg).

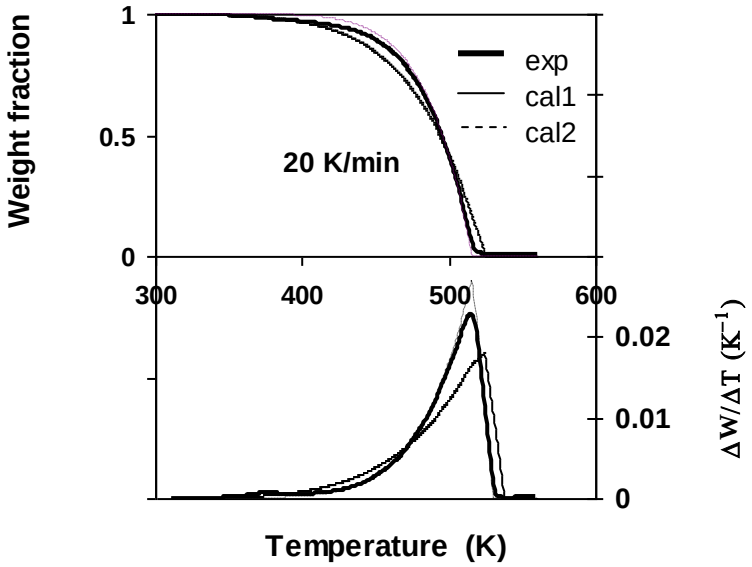

Figure 2. Experimental and calculated data for TG and DTG in N_2 atmosphere (sample mass:9 mg, 20 K/min)

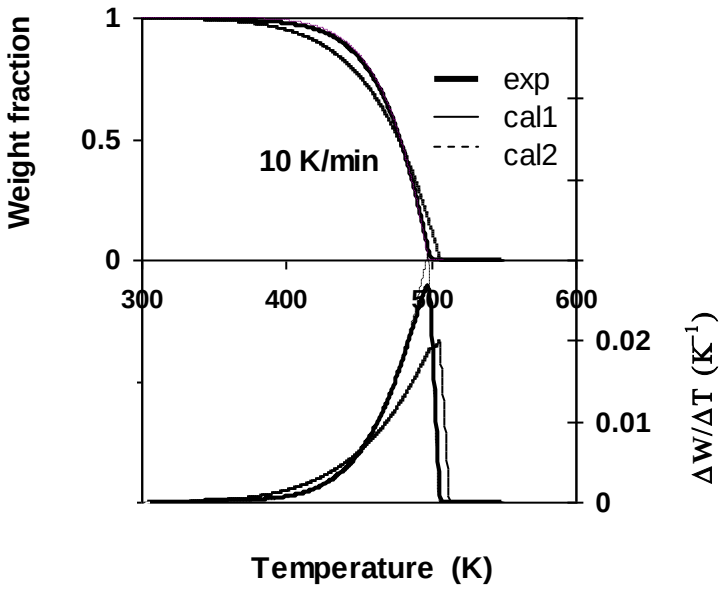

Figure 3. Experimental and calculated data for TG and DTG in N_2 atmosphere (sample mass: 9 mg, 10 K/min)

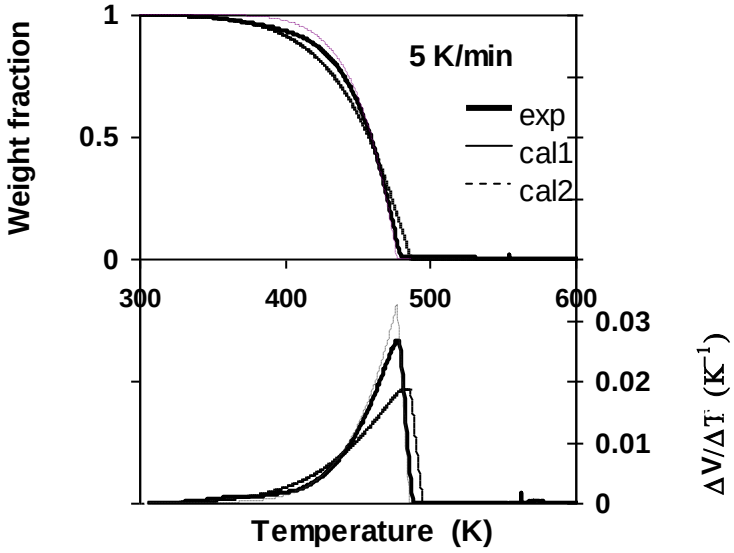

Figure 4. Experimental and calculated data for TG and DTG in N_2 atmosphere (sample mass: 9 mg, 5 K/min)

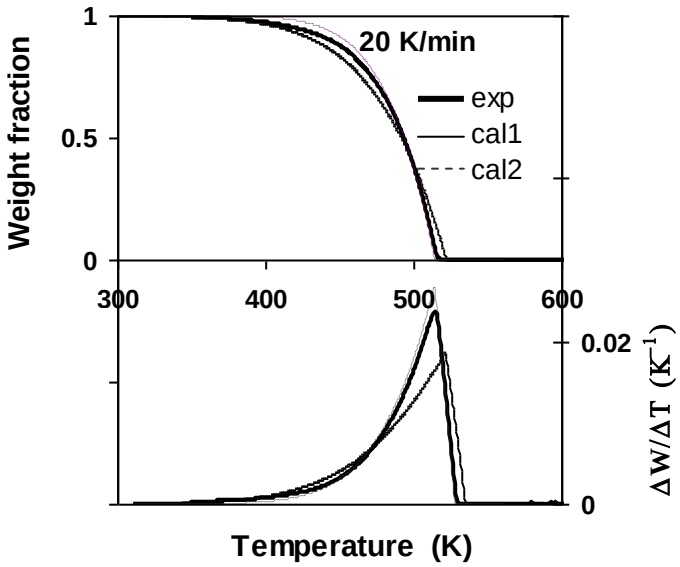

Figure 5. Experimental and calculated data for TG and DTG in air atmosphere (sample mass: 9 mg, 20 K/min)

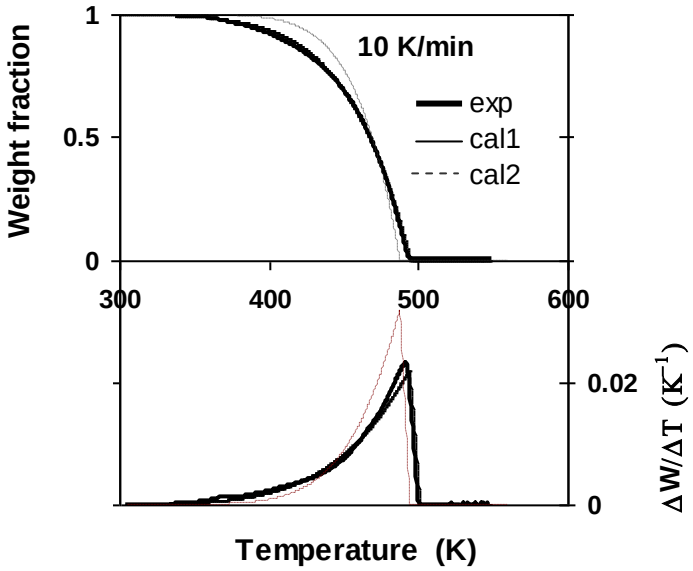

Figure 6. Experimental and calculated data for TG and DTG in air atmosphere (sample mass: 9 mg, 10 K/min)

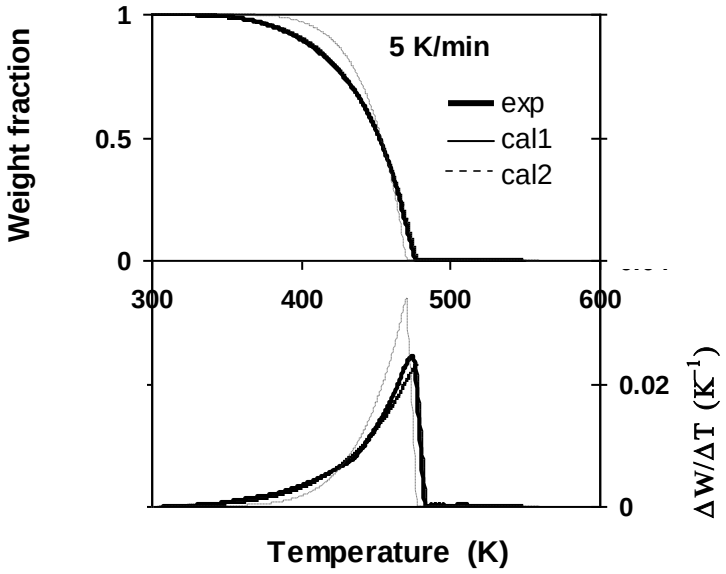

Figure 7. Experimental and calculated data for TG and DTG in air atmosphere (sample mass: 9 mg, 5 K/min)

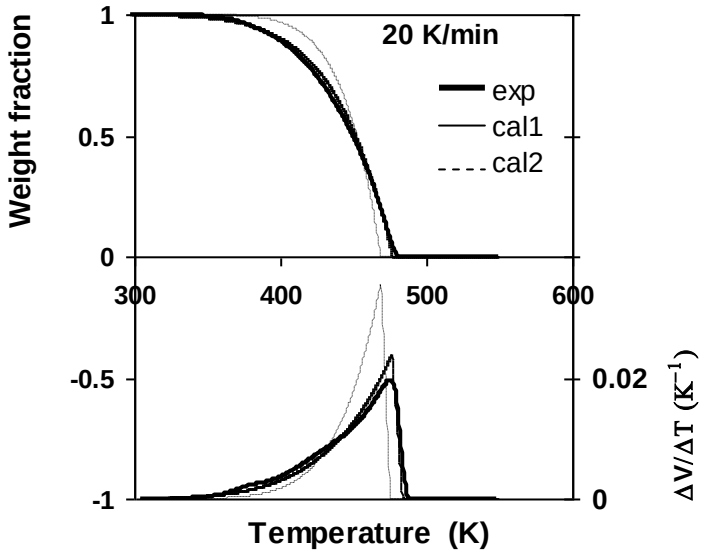

Figure 8. Experimental and calculated data for TG and DTG in N_2 atmosphere (sample mass: 5 mg, 20 K/min)

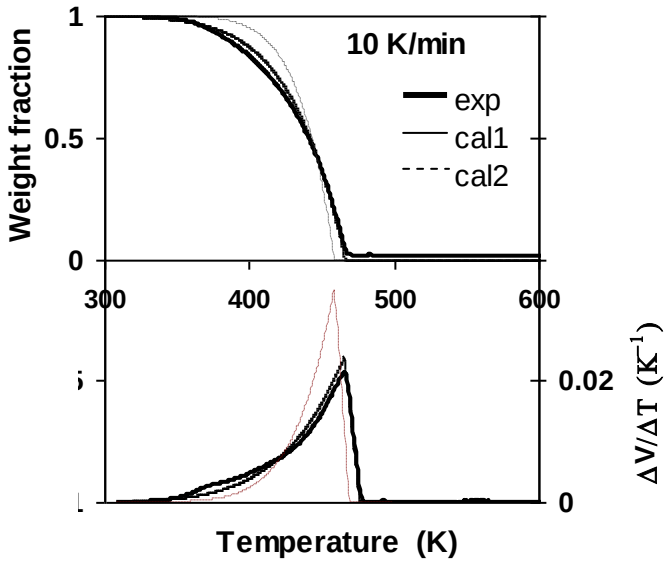

Figure 9. Experimental and calculated data for TG and DTG in N_2 atmosphere (sample mass: 5 mg, 10 K/min)

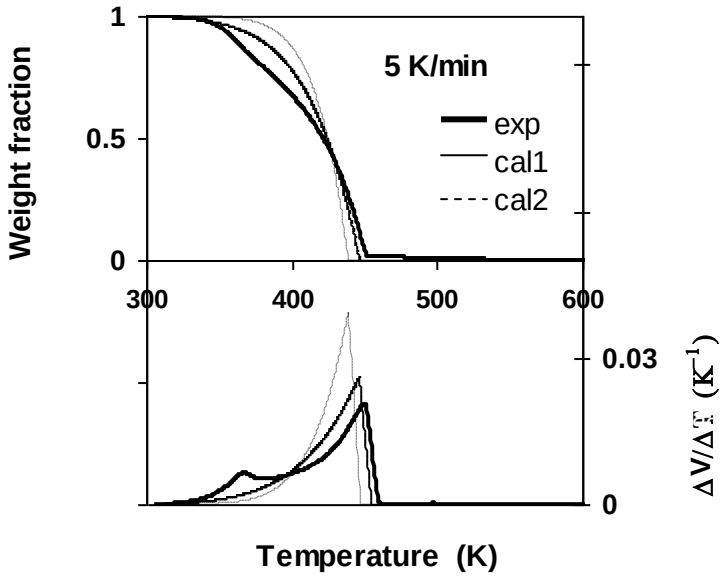

Figure 10. Experimental and calculated data for TG and DTG in N_2 atmosphere (sample mass: 5 mg, 5 K/min)

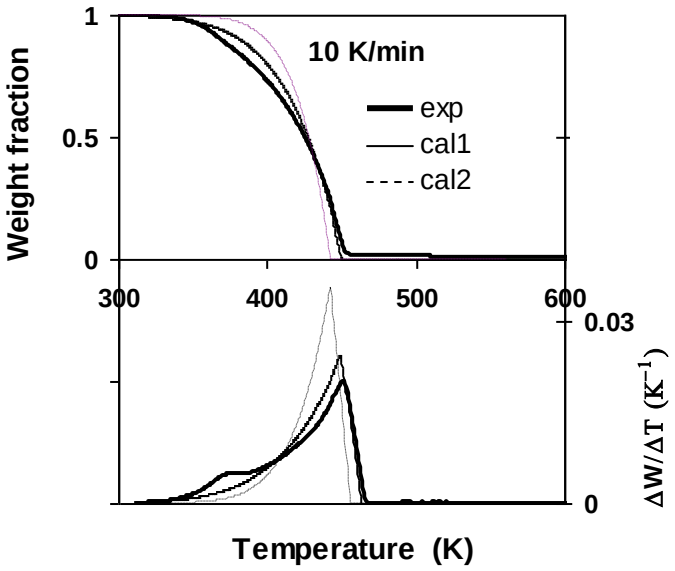

Figure 11. Experimental and calculated data for TG and DTG in N_2 atmosphere (sample mass: 2.5 mg, 10 K/min)

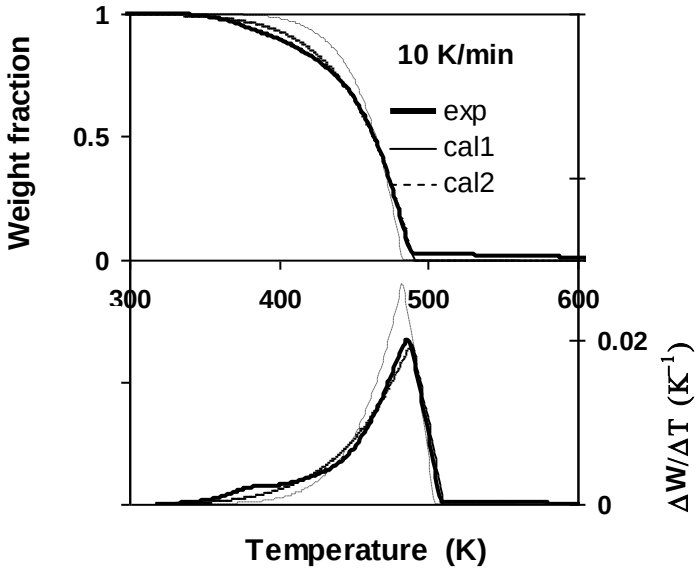

Figure 12. Experimental and calculated data for TG and DTG in N_2 atmosphere (sample mass: 7.5 mg, 10 K/min)

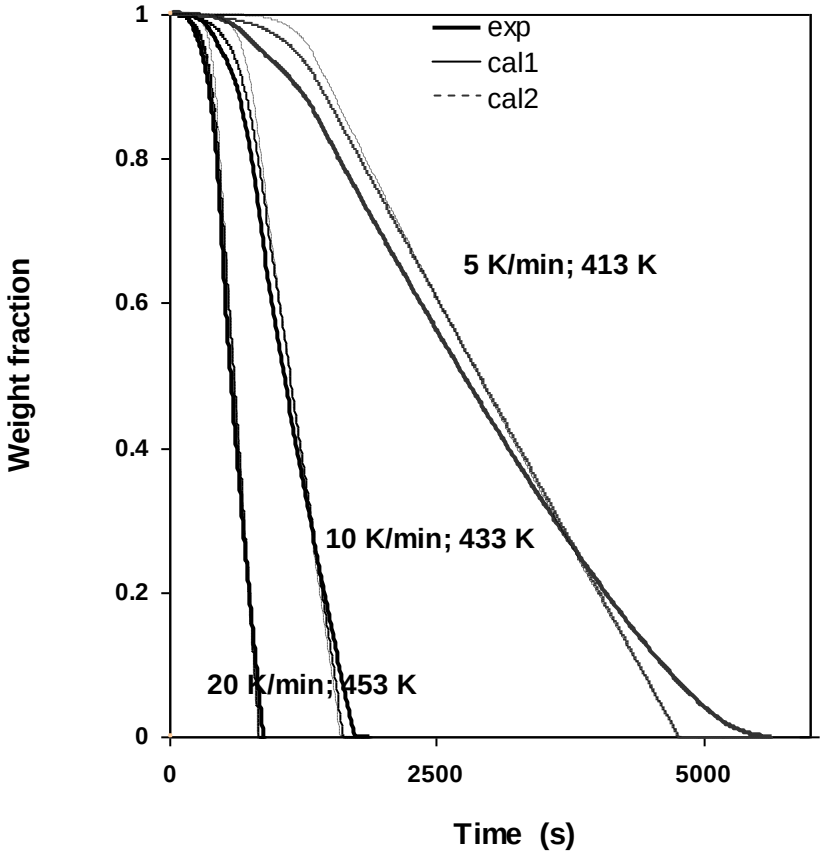

Figure 13. Experimental and calculated data for isothermal runs in N_2 atmosphere (sample mass: 9 mg)

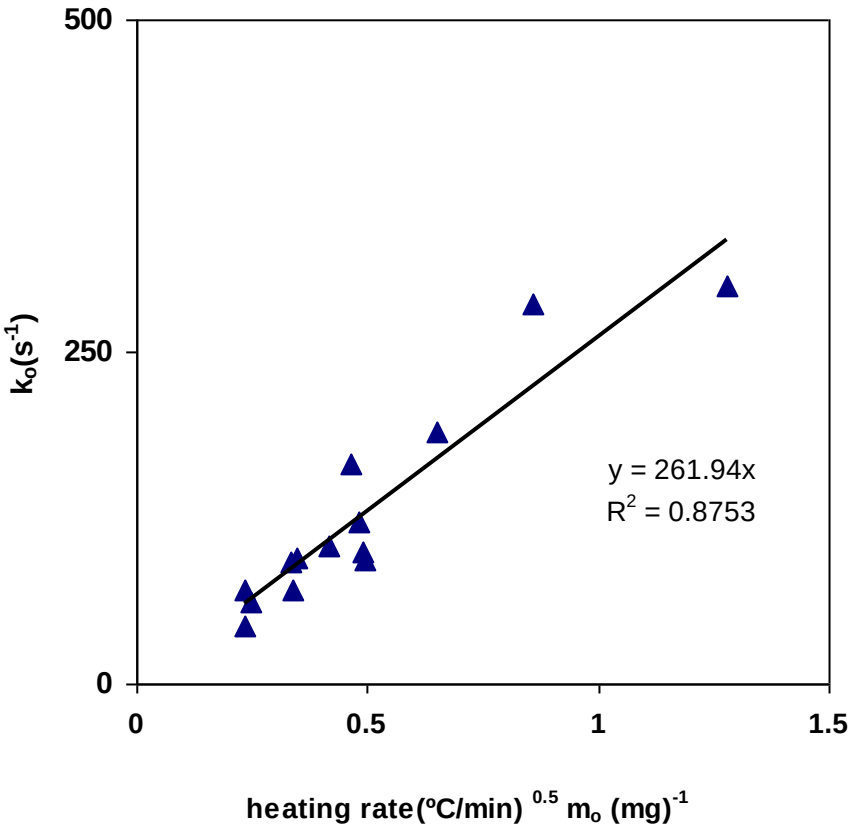

Figure 14. Variation of the pre-exponential factor vs. initial mass and heating rate

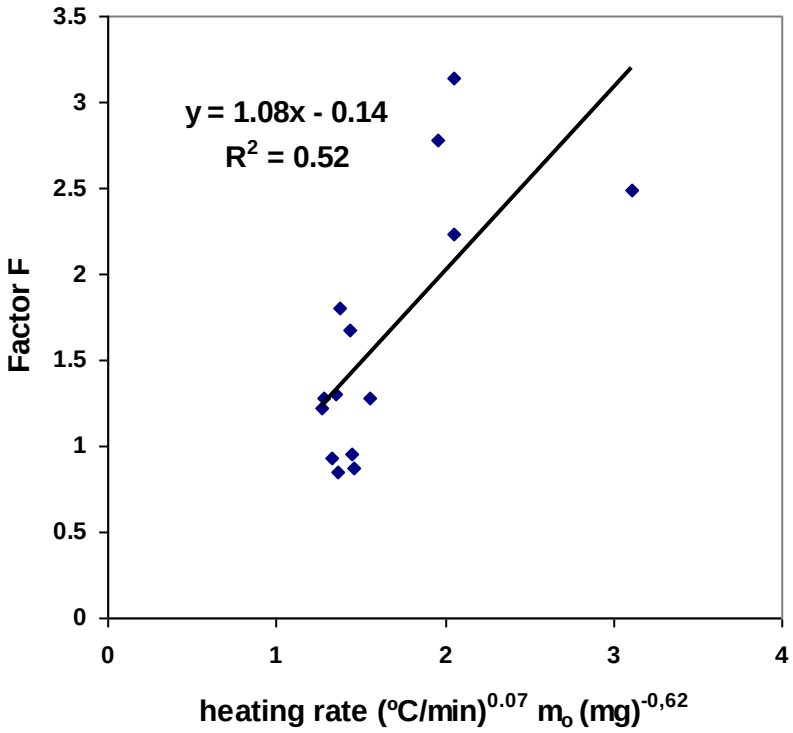

Figure 15. Variation of the factor F vs. heating rate and initial mass

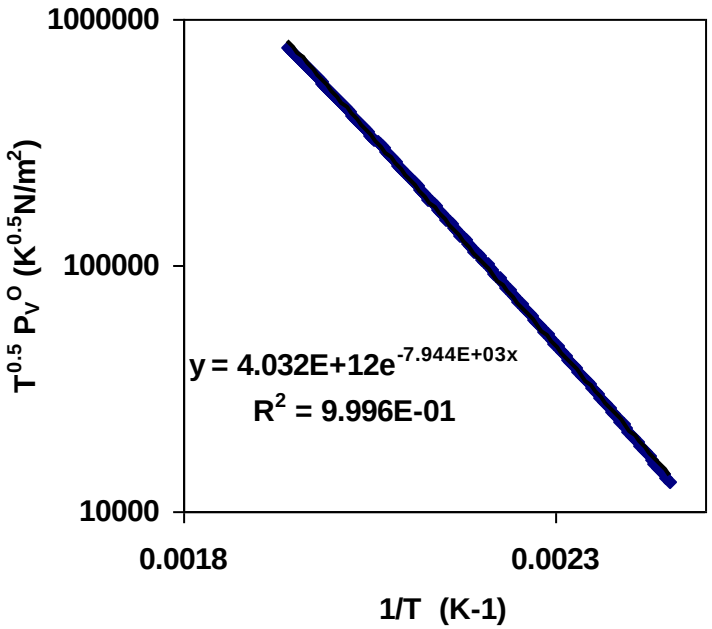

Figure 16. Variation of $T^{0.5}P_v^o$ vs. 1/T.

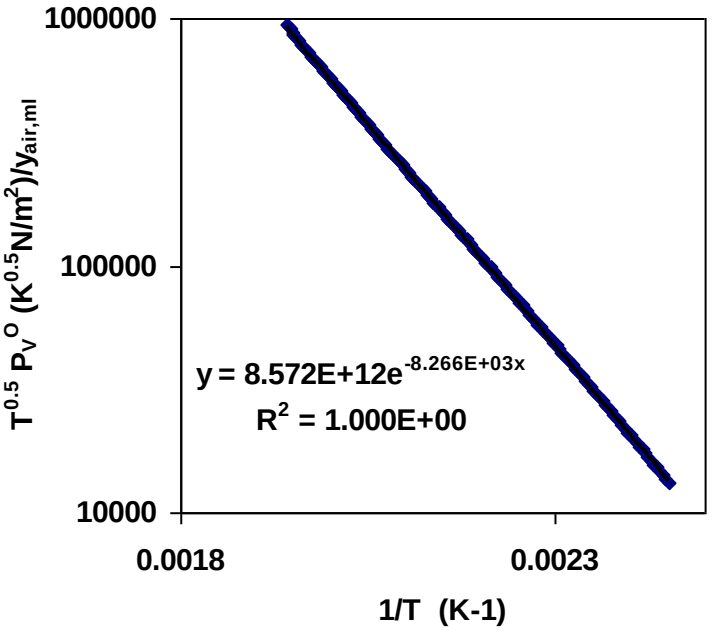

Figure 17. Variation of $T^{0.5}P_v^o$ /$y_{air,ml}$ vs. 1/T.